JOURNAL OF MATERIALS SCIENCE 21 (1986) 2339–2346

Time-independent mechanical properties of a chromium–manganese austenitic steel weldment

G. PIATTI, G. MUSSO
Materials Science Division, Commission of the European Communities, Joint Research Centre, Ispra Establishment, I-21020 Ispra (Varese), Italy

Room and elevated (450° C) temperature tensile data and room temperature notch impact data on weld metal and a welded joint of 10 wt % Cr–17.5 wt % Mn austenitic steel, a candidate material for thermonuclear fusion reactor first wall and blanket structures, are reported and discussed in terms of the microstructural features observed.

1. Introduction

Chromium–manganese steels (nickel-, molybdenum- and niobium-free grades) are of interest for use in thermonuclear fusion reactor first wall and blanket structures because of low long-term activation which is lower than that of type 316 stainless steel [1, 2]. This family of steels has been investigated in different laboratories in order to characterize and optimize structural and mechanical behaviour in non-irradiated and irradiated conditions [3–10]. However, although high manganese steels show improved welding characteristics [11, 12], only a few results related to physical and mechanical properties of weldments are reported in the literature [13].

The present paper deals with work carried out on the time-independent mechanical behaviour of a weld joint of 10Cr–17.5Mn (Ni-free grade) austenitic steel plates realized with a shielded metal arc welding process using a flux-covered consumable electrode of composition similar to the base metal. Thus the properties of the joint can match those of the metal joined. The time-independent properties were determined by room and high (450° C) temperature tension tests and room temperature Charpy V-notch impact tests on small specimens taken from weld metal, heat affected zones and base metal regions of the arc-welded joint. Factors influencing the mechanical weldment behaviour were studied by optical and scanning electron microscopy.

Time-dependent (creep and creep fatigue) tests were not considered because in the temperature range which is of interest in the first wall service conditions, and which extends up to approximately 450° C [14], time-independent tests are sufficient to describe the AMRC 0033 alloy with respect to design and safety analysis considerations for potential fusion reactor applications. In this material, in fact, time-dependent behaviour becomes significant from 500° C (the temperature at which there is superposition with the time-independent behaviour) and becomes dominant above 550° C [15].

2. Materials

The material selected for the present study was the experimental AMCR 0033–Creusot-Loire steel, (France) supplied as 30 mm thick solution annealed plate and was used by the authors in the as-received conditions. Its chemical analysis is given in Table I. It should be observed that the material concerned included a relatively high amount of carbon (0.1 wt %) and nitrogen (0.2 wt %), the composition being balanced to avoid the ε(h c p) and α'(b c c) martensite phases and to stabilize the γ(f c c) austenitic phase. In fact, because the manganese is not as powerful a γ stabilizer as nickel, the interstitial element additions listed in Table I are necessary to lower the $M_s(\varepsilon)$ and $M_s(\alpha')$ points below the room temperature [16] $M_s(\varepsilon)$ and $M_s(\alpha')$ being the upper temperature at which the ε(h c p) and the α'(b c c) martensite, respectively, begin to form spontaneously from austenite on cooling. However, in the AMCR 0033, during deformation at room temperature, $\gamma \rightarrow \varepsilon$ transformations can occur with a considerable increase of the strain hardening rate [5].

3. Experimental techniques

The welding procedure applied in this study, as previously mentioned, was a shielded metal-arc electrode having a core composition (Table II) similar to that of the base metal. The diameter of the core wire was 4 mm and the flux-cover was of the rutile-basic type. The choice of this electrode was made after a series of selection trials with different candidate electrodes by testing the sensitivity to hot cracking in the

TABLE I Chemical composition (wt %) of alloy studied (AMCR 0033-CREUSOT Loire)

Cr	Mn	Ni	Si	C	N	P	S	Mo	Cu	Al	Pb	B	Fe
10.09	17.37	< 0.10	0.55	0.095	0.195	0.020	0.009	< 0.065	< 0.060	< 0.005	1 p.p.m.	25 p.p.m.	balance

0022–2461/86 $03.00 + .12

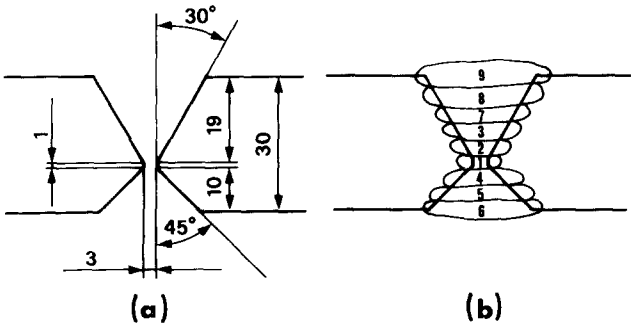

Figure 1 Details of the weld process: (a) shape and dimensions (mm) of the asymmetric double-V groove profile; (b) sequence of weld passes.

weld deposit by the FISCO test (Italian standard regulation UNI 8096). The assembly consisted of two plates (dimensions 2000 mm × 250 mm × 30 mm) joined along the longest side. The joint configuration, an asymmetrical double-V groove, is shown in Fig. 1a. A multipass procedure was adopted because of the thick section (30 mm) and the sequence of build-up operations is presented in Fig. 1b. An interpass temperature lower than 200° C was maintained and the plates were mechanically restrained during welding. The welded joint was checked by non-destructive testing techniques (fluorescent penetrant liquid method and radiography) prior to tensile specimen machining. A satisfactory weld soundness was found. No defects such as incomplete fusion, shrinkage or inclusions were encountered. However, because of the poor inspectability of the austenitic steels, it is difficult to detect such defects as microporosities and they could be present. No post-weld heat treatment was performed. The details of welding and post-welding procedure have been given elsewhere [17].

TABLE II Chemical composition (wt %) of filler metal and shielded metal-arc weld deposit

	Cr	Mn	Ni	Si	C	N	P	S	Fe
Filler metal	10	17	0.1	–	0.30	–	–	–	balance
Weld deposit	13.63	17.69	0.03	–	0.37	0.05	–	–	balance

Several round tensile specimens (diameter 4 mm and gauge length 20 mm) were machined from the welded joint with the tensile axis parallel to the weld axis. The sampling map is shown in Fig. 2. Some flat specimens (section 25 × 12 mm) with the tensile axis transverse to the weld axis were also machined. Tensile tests were performed at a strain rate of $10^{-3}\,sec^{-1}$ at room temperature and at 450° C on the longitudinal-to-weld specimens but only at room temperature on the transverse specimens. Moreover, standard 10 mm × 10 mm cross-section Charpy V-notch (CVN) samples were machined at different locations: (a) all weld metal near core; (b) all weld metal near surface; (c) transverse to weld metal; (d) all parent metal in a direction parallel to the weld axis, and were notched (10 mm × 8 mm cross-section) perpendicular to the weld surface. Impact tests were performed at room temperature.

Transverse sections cut from the welded joint and transverse and longitudinal specimens taken from selected deformed tensile specimens, were prepared by mechanical polishing and electrochemical etching for observation with optical and scanning electron microscopes (Philips SEM 505). Great care must be taken during the polishing stage because this steel is susceptible to work hardening [5] and surface deformation, and consequently to the development of layers of disturbed metal. SEM analysis was also employed to investigate the fracture surface of some

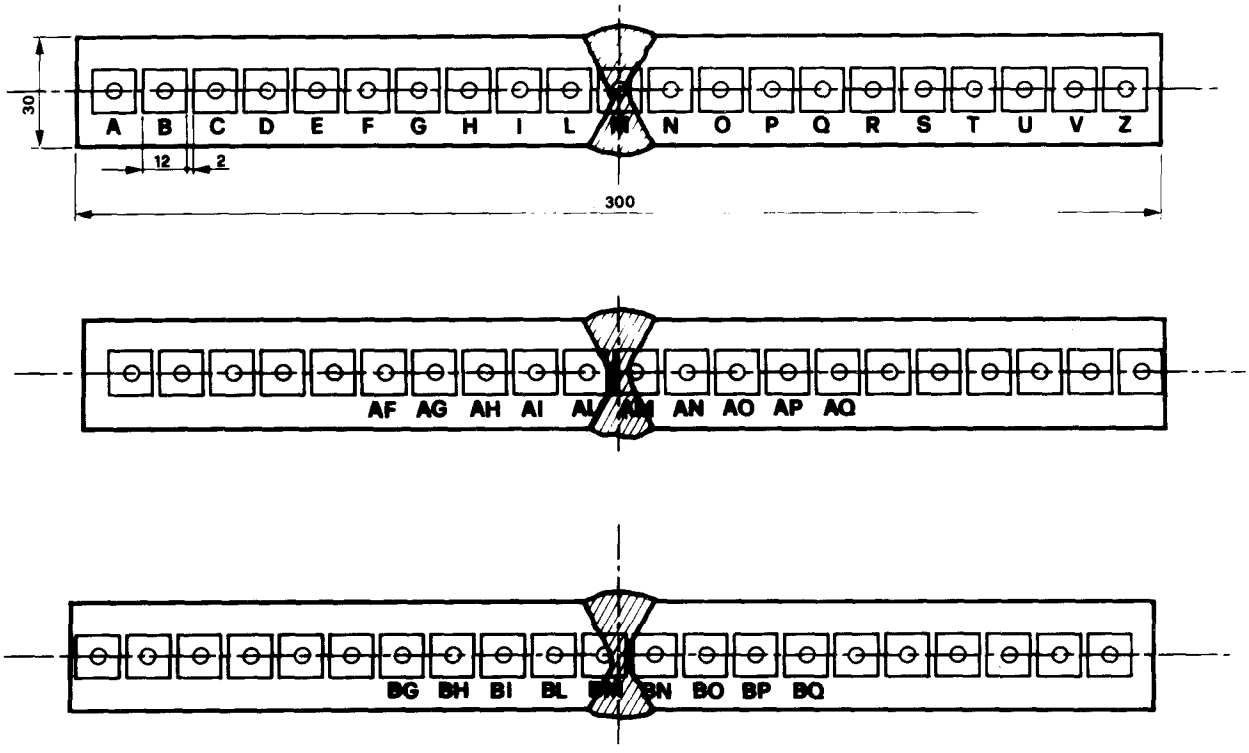

Figure 2 Sections of welded joint of 10Cr–17.5Mn austenitic steel plates showing sampling location of longitudinal-to-weld specimens. Shaded area represents weld metal. Dimensions in millimetres.

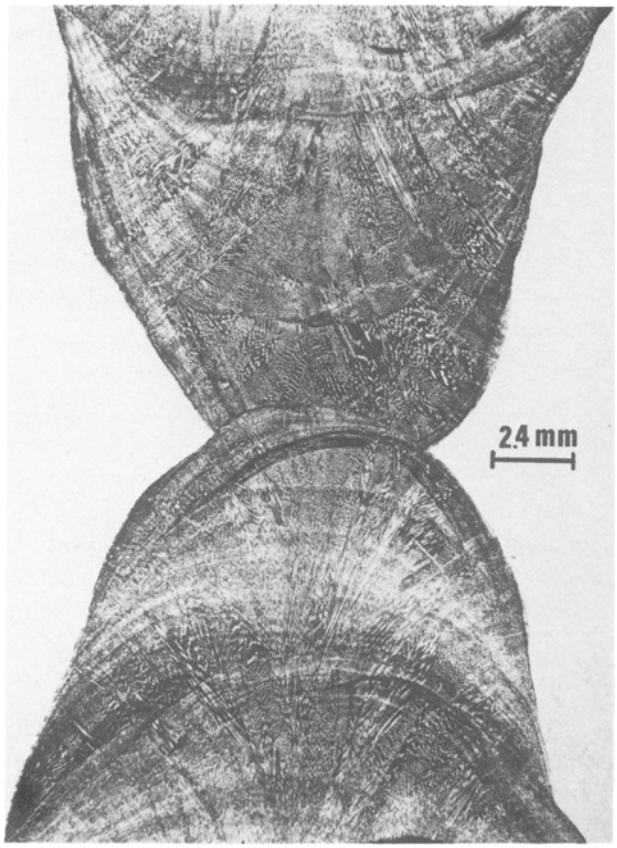

Figure 3 Optical micrograph of a section of welded joint of 10Cr–17.5Mn austenitic steel plates.

broken tensile specimens. Finally, the effects of microstructural changes were assessed by micro-hardness tests made on the transverse sections from the welded joint.

4. Results and discussion

4.1. Welding characteristics

The welding characteristics were satisfactory and were comparable from a general point of view to those of other austenitic stainless steels. In fact, the welds showed good wetting, sidewall fusion and liquid penetration. This means that the working pool of molten metal created by the shielded arc welding process was able to solidify within the joint by epitaxial nucleation and growth from existing solid interfaces. These features are seen in Fig. 3 which shows a micrograph of a section of the welded joint. 10Cr–17.5Mn austenitic steel can hence be considered as weldable.

4.2. Microstructures

The fully γ-austenitic structure of the base metal (as-received) according to previous studies on this steel [4, 5] is shown in Fig. 4a. A typical f c c annealed structure, i.e. randomly oriented grains which present twinning, is evident. A mean grain size of $70 \pm 10\,\mu m$ was measured [5]. There is also the presence of non-metallic inclusions such as MnS and Al_2O_3 but there is no evidence of carbide precipitation [4]. The weld metal is also fully austenitic, according to preliminary microstructural observations performed by Ruedl and co-workers and published elsewhere [16] and according to the Schaeffler diagram [18], which shows the phase fields in terms of the nickel and chromium equivalents, specially modified for Cr–Mn steel [19]. The weld material presents an as-cast type structure (Fig. 4b) with a dendrite morphology. Moreover, it should be mentioned that the segregation phenomena which invariably occur during the solidification

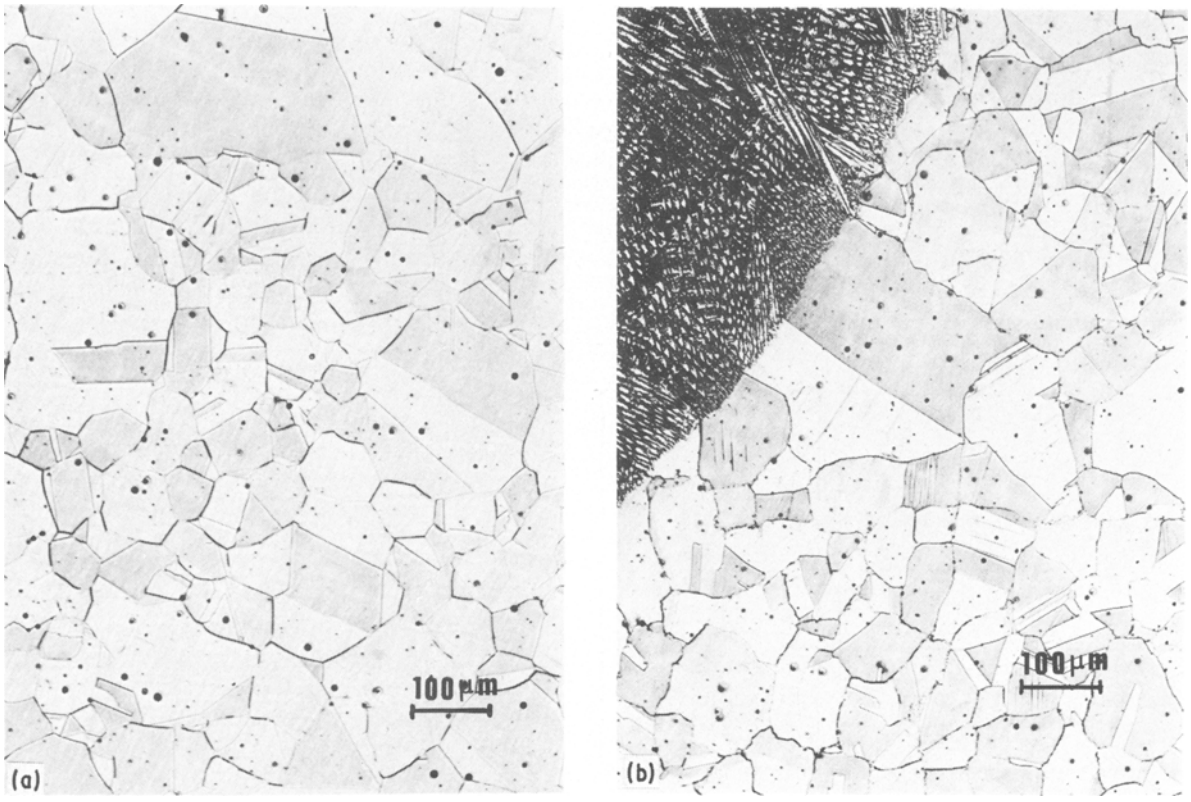

Figure 4 Microstructure of the welded joint of 10Cr–17.5Mn austenitic steel plates: (a) base metal, (b) fusion and heat-affected zones.

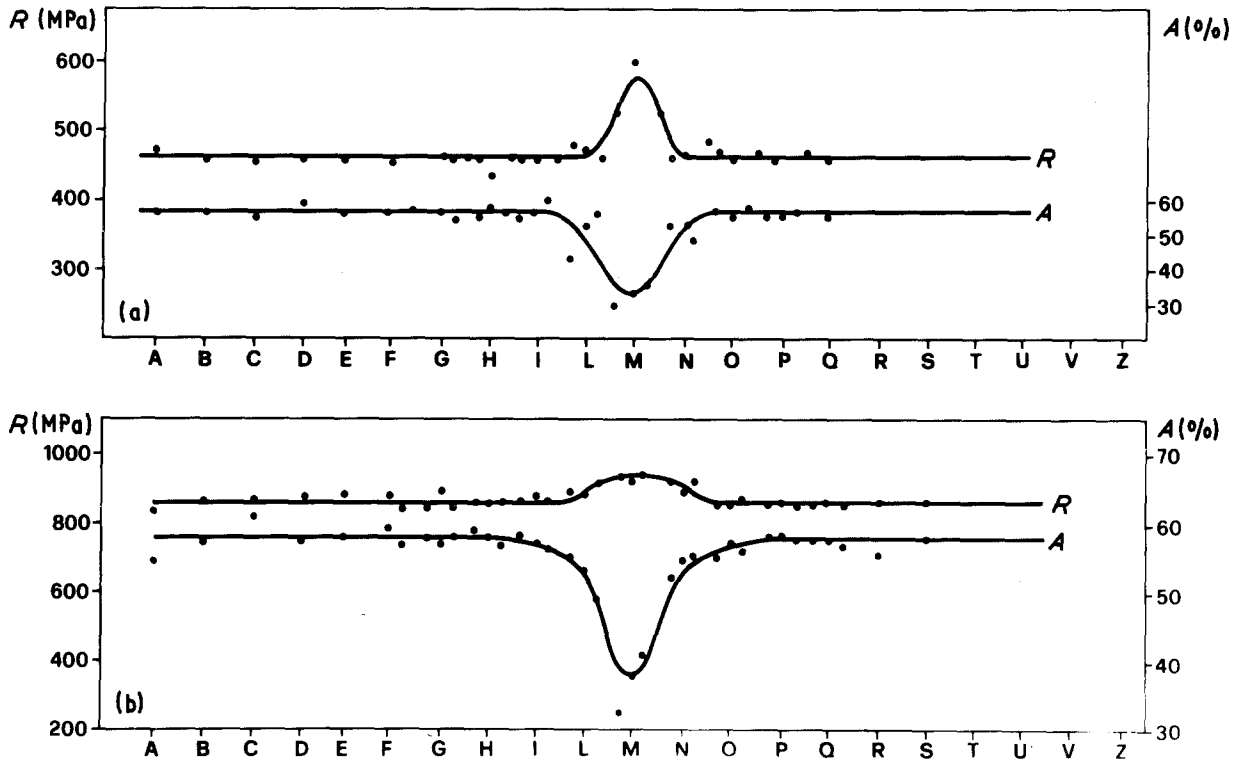

Figure 5 Plot of tensile characteristics: ultimate tensile strength (R) and total elongation (A), determined at (a) room temperature and (b) at 450° C, against sampling location. For reason of clarity, samples AF, AG, etc. (see Fig. 2) are not indicated.

process are particularly significant in iron alloys with a high percentage of manganese and are difficult to avoid [20, 21]. Carbide precipitation in the fusion zone, due to the high carbon-content (0.37 wt %), was detected. The usual heat input limitations were not sufficient to avoid this phenomenon which is also present in the heat-affected zone. The latter is not fully austenitic because of the presence of a certain amount of strain-induced ε martensite due to thermal and mechanical cycling occurring in the region near the weld during the welding process. This feature is in agreement with observations of martensitic transformation during room temperature deformation of AMCR 0033 [5] as previously mentioned. Moreover, the results show an appreciable austenite grain coarsening.

4.3. Mechanical properties

The results (Fig. 5) related to tensile tests performed on longitudinal-to-weld specimens, taken in different positions according to the map of Fig. 2, show that the specimens from the heat-affected zone (L, AL and BN, for instance) and from the fusion zone (M) differ significantly in their behaviour from specimens from unaffected zone regions of the weld (A, AF and BG, for instance). The tensile strength of the weld metal is increased by 10% at room temperature and 30% at 450° C of the tensile strength of the base metal, whereas the ductility of the weld metal is strongly reduced to 60% of that of the parent metal at both the temperatures investigated. The weld metal and the metal near to the fusion zone were then found to be stronger than base metal.

Clearly, probably a solid solution hardening effect occurs because of the high interstitial carbon content [22] (C = 0.37%, see Table II) in the weld metal, and also near to the fusion zone due to diffusion processes operating during welding. Moreover, there may be also an appreciable contribution to the hardening due to the probably higher dislocation density on the fusion zone and especially in the core, as shown for type 316 stainless steel [23]. It should be mentioned that the 0.2 yield strength (not plotted in Fig. 5 for reasons of clarity) of the weld and of the HAZ zone were also above those of parent metal.

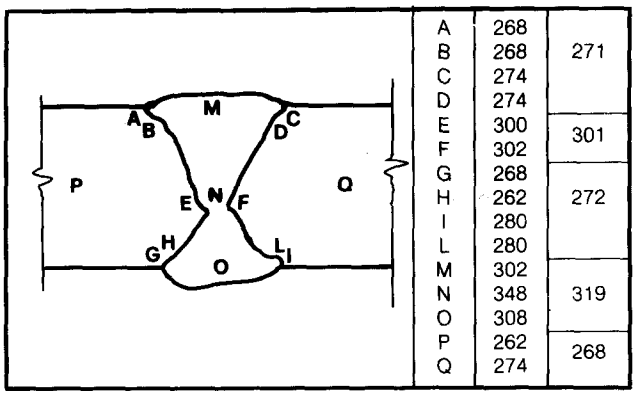

Figure 6 Hardness distribution (HV 30) in a section of the welded joint of 10Cr–17.5Mn austenitic steel plates.

TABLE III Charpy V-notch impact data

Sample location	Resilience* ($J cm^{-2}$)
All weld metal near to core	73
All weld metal near to surface	108
Transverse to weld metal	161
All base metal with specimen axis parallel to weld axis	254

*Average values.

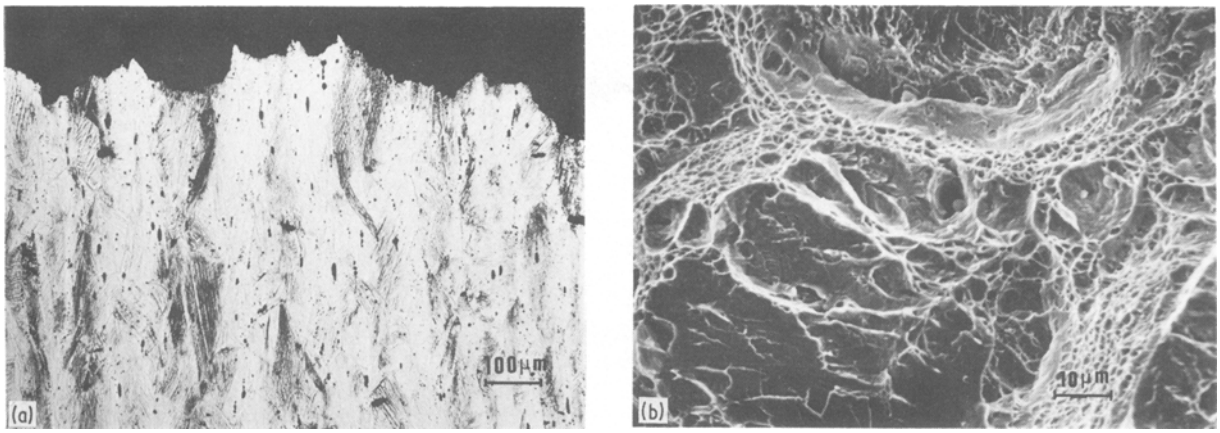

Figure 7 Tensile specimen (B, see Fig. 2) taken from the base metal deformed at room temperature: (a) longitudinal section (optical micrograph), and (b) fracture surface (SEM image).

This hardening effect is shown in Fig. 6 showing the Vickers hardness measurement (HV 30) in a transverse section of the welded joint. There is a considerably difference between Vickers hardness numbers corresponding to the base metal (average value 268) and those corresponding to the inside of the weld (average value 319) where the amount of carbon is higher.

Fig. 5 also shows that the weld metal is less ductile than the base metal at both the temperatures investigated. Presumably the segregation phenomena mentioned, which occur on the fusion weld zone, induce inhomogeneities and migration of impurities in the grain boundaries and inside the grains with a negative but not serious effect on the rupture elongations of the weld; the minimum values reported are still at a relatively high level, greater than a ductility of 30%.

Concerning the transverse-to-joint specimens results, a tensile strength average value (735 MPa) lower than that (860 MPa from Fig. 5a) of base metal and also than that (940 MPa from Fig. 5a) of the welded metal was obtained. This behaviour can be expected with composite type specimens. A complex geometrical restraint, because of the different deformation resistances of the various zones of the weld occurs and can influence their response to deformation. It is interesting to note that the fracture position was in the weld metal.

The results concerning the Charpy V-notch impact tests (Table III) show that the toughness properties of the weld metals are different from those of base metal as was the case for the tensile properties. More precisely the weld presents an average energy absorption value (73 to 108 J cm^{-2}) lower than that of the base metal (254 J cm^{-2}). However, according to various toughness data evaluations of Fe–Cr–Mn alloys [20], the Charpy V-notch impact data measured near to the core (73 J cm^{-2}) is to be considered satisfactory and the data measurement near to the surface (108 J cm^{-2}) excellent. The average value relating to transverse-to-weld metal specimens (161 J cm^{-2}) can also be classified as excellent. Thus the welded joint has a low notch sensitivity.

4.4. Fracture

The results are summarized in Figs 7 to 12, Figs 7 and 8 referring to the base metal broken specimens (B, see Fig. 2), Figs 9 and 10 to the heat-affected zone broken specimens (BM, see Fig. 2) and Figs 11 and 12 to fusion zone broken specimens (M, see Fig. 2). In the base metal two deformation processes (slip plus martensite) occur at room temperature (Fig. 7a) as previously observed in this material [5]. ε-martensite volume fraction was assessed in the fracture zone as $\sim 50\%$ whereas a low component ($\sim 10\%$) of α'-martensite was also found [16]. The fracture profile

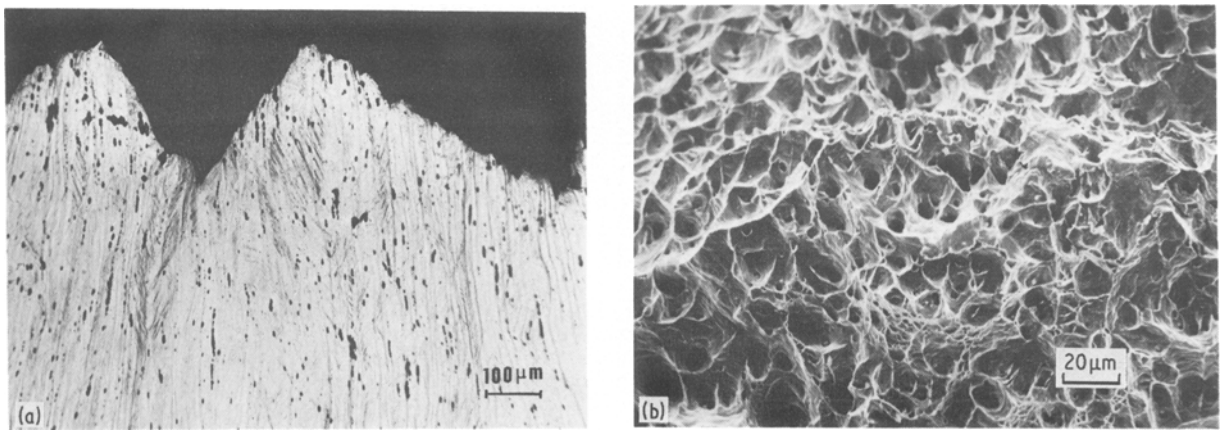

Figure 8 Tensile specimen (B, see Fig. 2) taken from the base metal deformed at 450° C: (a) longitudinal section (optical micrograph), and (b) fracture surface (SEM image).

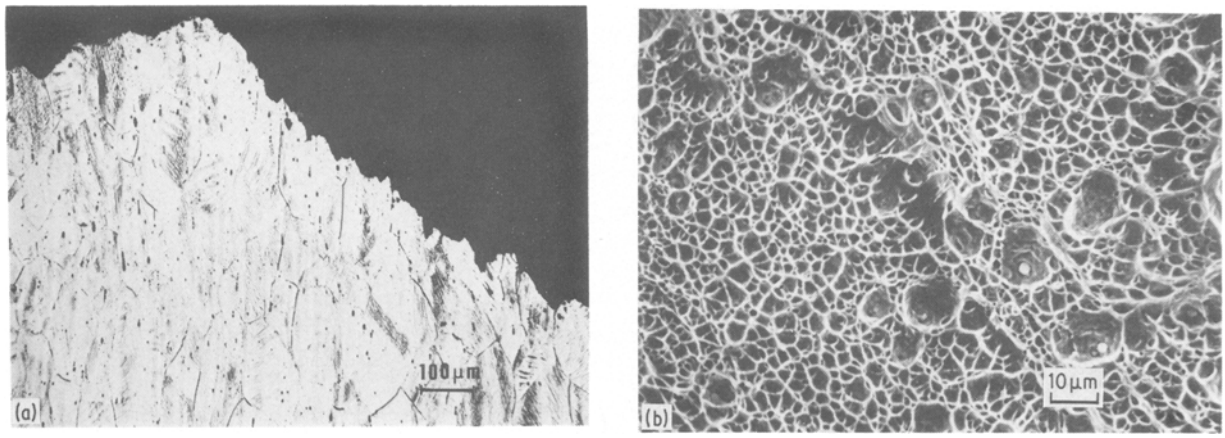

Figure 9 Tensile specimen (BM, see Fig. 2) taken from the heat-affected zone deformed at room temperature: (a) longitudinal section (optical micrograph), and (b) fracture surface (SEM image).

(Fig. 7a) shows a premature failure without necking characterized by a transgranular fracture surface of mixed (brittle plus ductile) appearance (Fig. 7b). In fact, cleavage and microvoids occur. However, it should be observed that the strain-induced $\gamma \rightarrow \varepsilon$ transformation, even if responsible for the partially brittle appearance of the fracture surface of the base metal broken specimens, does not exclude the occurrence of the large elongation at rupture values (60% from Fig. 5) according to a mechanism typical of the TRIP steels, as was proposed previously [5, 20]. At 450° C the deformation occurs by slip processes and there is no evidence of martensite formaton (Fig. 8a). The fracture is completely ductile and there is a large range of dimple sizes (Fig. 8b).

In the heat-affected zone broken specimens, martensite is also manifest but only near to the fracture (Fig. 9a) where the deformation is more important. In fact, the higher level of carbon in the heat-affected zone, because of the diffusion process operating during the welding procedure, stabilizes the γ-phase and prevents the strain-controlled $\gamma \rightarrow \varepsilon$ transformation. The fracture (Fig. 9a) presents a shear rupture profile and the fracture surface shows a ductile (dimpled) transgranular surface (Fig. 9b). At 450° C only a slip deformation process occurs and the fracture is completely ductile from a macroscopic point of view (cup and cone profile, Fig. 10a) and from a microscopic point of view (shear dimples, Fig. 10b). This can be seen from the void nucleation, growth and coalescence micromechanism characteristic of the dimple fracture. In the fusion zone broken specimens the fracture profile shows no necking (Fig. 11a) and the fracture zone shows dimples but with some localized cleavage (Fig. 11b). Microvoids begin at the interface between the matrix and the particles (including carbides) and also at imperfections such as secondary microcracks. The several inclusions and precipitates are trapped between the dendrite branches. The fracture behaviour is then clearly less ductile than in the base metal and heat affected zone. At 450° C (Fig. 12a) the behaviour is similar to that at room temperature but a higher degree of ductility can be seen (Fig. 12b). In conclusion concerning fracture, there is a significant variation in the failure process depending on the sampling location of the tensile specimens, especially at room temperature.

4.5. Design implications

The room and high temperature weldment behaviour of 10Cr–17.5Mn austenitic steel is characterized by the different inelastic properties of the base metal and of the weld metal. It follows that this must have some implications for the design and safety considerations

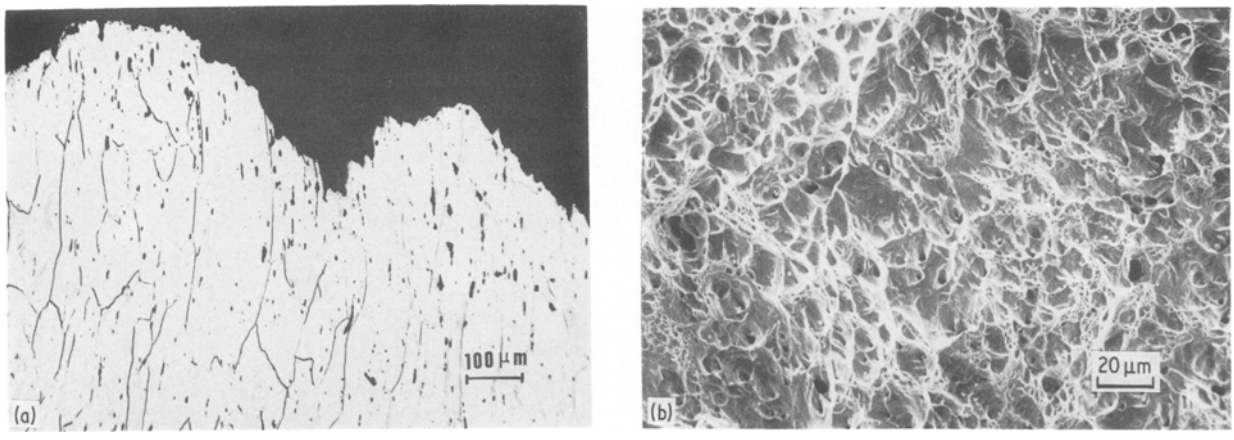

Figure 10 Tensile specimen (BM, see Fig. 2) taken from the heat-affected zone deformed at 450° C: (a) longitudinal section (optical micrograph), and (b) fracture surface (SEM image).

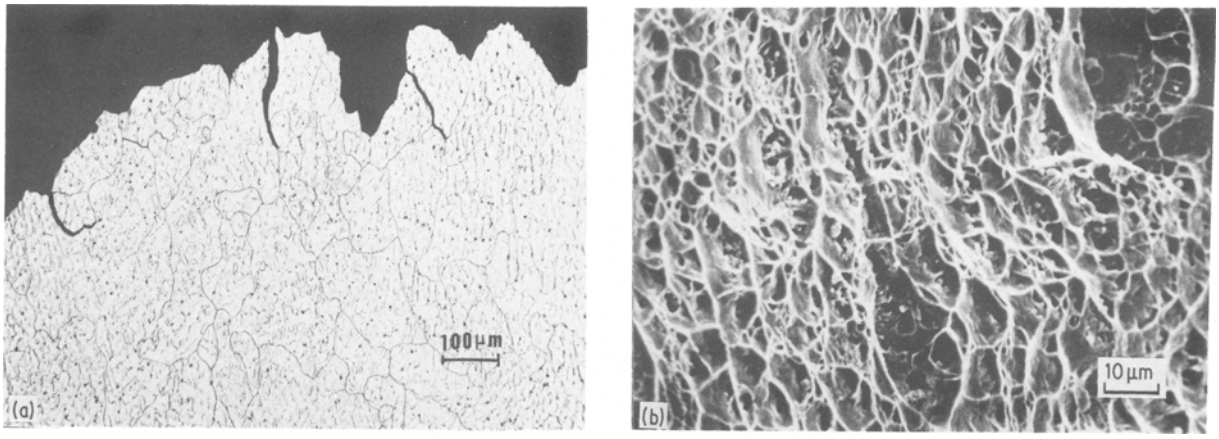

Figure 11 Tensile specimen (M, see Fig. 2) taken from the fusion zone and deformed at room temperature: (a) longitudinal section (optical micrograph), and (b) fracture surface (SEM image).

of this potential material candidate for fusion reactor components. Generally a design stress factor, f, is obtained by dividing the strength of the weakest zone of the welded joint by the strength of the parent metal. Because of the tensile strength and 0.2 yield strength weld region values higher than those of parent metal, a design stress factor 1 can be assumed. However, the design stress factor method does not consider reduced ductility values in individual points of welds, which are possible in this case because of the acceptable, but not very high, mean value of the welded zone ductility. Hence, it is preferable to consider a strain base design concept with a reduction factor based on strain values. The ASME CC N47 assumes the design strain for the welded joint as half the allowable value for base metal.

5. Conclusions

1. The 10Cr–17.5Mn austenitic steel can be considered as weldable with a shielded metal-arc process and with a flux-covered consumable electrode of composition similar to the base metal.

2. The room and 450° C weldment behaviour of 10Cr–17.5Mn austenitic steel is influenced by the different inelastic properties of the base metal and of the weld metal.

3. The weld metal and the metal near to the fusion zone are stronger than the base metal but are less ductile.

4. A strong solid solution hardening effect occurs in the weld metal because of the high interstitial carbon content (C = 0.37 wt %) of the consumable electrode.

5. Results concerning the transverse-to-weld specimens show that the tensile strength average value (735 MPa) is inferior to that of base metal (860 MPa).

6. The welded joints show a low notch sensitivity.

Acknowledgements

The welding process was performed by the Istituto Italiano della Saldatura of Genoa (Italy) with the supervision of C. Masetti. Thanks are also due to Dr P. Schiller, Dr E. Ruedl and Dr D. G. Rickerby for helpful discussions and critical comments, and to E. Haine, G. P. Ossola and H. P. Weir for experimental work. The present work was performed as part of the "Technology of thermonuclear fusion" programme of the JRC Ispra Establishment.

References

1. P. FENICI, D. BOERMAN, V. COEN, E. LANG, C. PONTI and W. SCHÜLE, *Nucl. Eng. Design/Fusion* **1** (1984) 167.
2. R. W. CONN, E. E. BLOOM, J. W. DAVIS, R. E. GOLD, R. LITTLE, K. R. SCHULTZ, D. L. SMITH and F. W. WIFFEN, *Nucl. Technol./Fusion* **5** (1984) 291.
3. G. PIATTI, S. MATTEAZZI and G. PETRONE, *Mém Etud. Sci. Rev. Metall.* **79** (1982) 794.

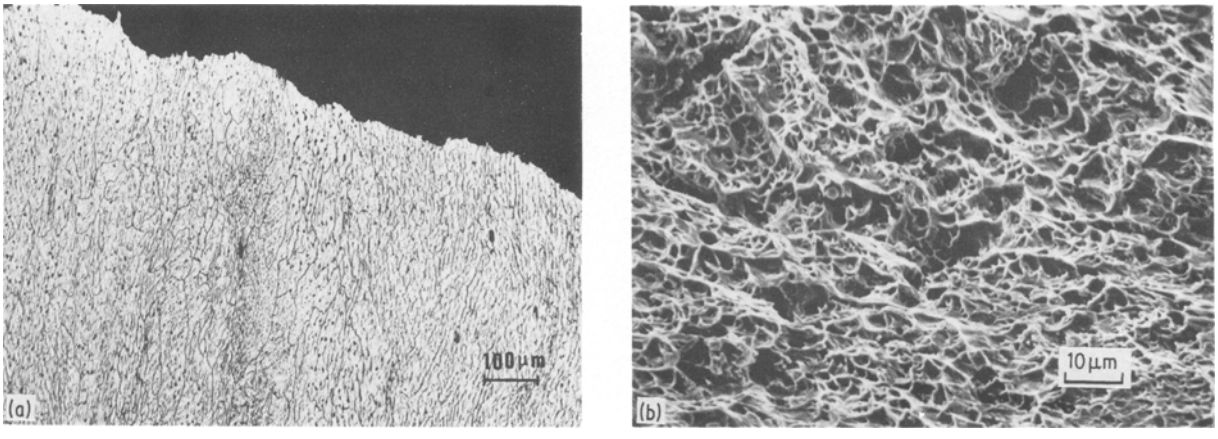

Figure 12 Tensile test (M, see Fig. 2) taken from the fusion zone and deformed at 450° C, (a) longitudinal section (optical micrograph), and (b) fracture surface (SEM image).

4. E. RUEDL and T. SASAKI, *J. Nucl. Mater.* **122** (1984) 794.
5. G. PIATTI, S. MATTEAZZI and G. PETRONE, *Nucl. Eng. Design/Fusion* **2** (1985) 391.
6. D. G. RICKERBY, T. SASAKI and E. RUEDL, in Proceedings of the 8th European Congress on Electron Microscopy, Budapest, August (1984), edited by A. Csanady, P. Röhlich and D. Szabo, p. 777.
7. M. SNYKERS and E. RUEDL, *J. Nucl. Mater.* **103, 104** (1981) 1075.
8. D. J. MAZEY, J. A. HUDSON and J. M. TITCHMARSH, *J. Nucl. Mater.* **107** (1982) 2.
9. H. R. BRAGER, F. A. GARNER, D. S. GELLES and M. L. HAMILTON, *J. Nucl. Mater.* **133, 134** (1985) 907.
10. R. L. KLUEH and M. L. GROSSBECK, *J. Nucl. Mater.* **122, 123** (1984) 294.
11. J. HOCHMANN, *Matér. Tech.*(December) (1977) 69.
12. W. T. DE LONG and H. F. REID, *Welding J.* **1** (1957) 41-S.
13. S. HORVATH, *Zvaranie* **18** (1969) 25.
14. INTOR Workshop, IAEA, Vienna, Report EURFUBRU/XII/1-8G-EDV10, CEC-BRUSSEL, January (1984).
15. G. BERNASCONI, S. MATTEAZZI, G. PETRONE and R. MATERA, oral presentation, 9th SMIRT, Brussels (1985) paper L2/8.
16. E. RUEDL, D. G. RICKERBY and T. SASAKI, in "Proceedings of the 13th SOFT", Varese, Italy (1984) (Pergamon Press, Oxford, 1984) p. 1029.
17. G. MUSSO, G. PIATTI AND C. MASETTI, Poster presentation to Journées Métallurgiques d'Automne, Paris (October, 1983).
18. A. L. SCHAEFFLER,M *Met. Progr.* **56** (1949) 680.
19. M. I. RAZIKOV, G. N. KOCHEVA and L. G. TOLSTYKH, *Avt. Svarka* **21** (1968) 1.
20. J. CHARLES, Thesis, Catholic University of Louvain, Louvain-la-Neuve, Belgium (1982).
21. H. SCHUMANN and K. GOODKNECHT, *Prakt. Metallogr.* **4** (1967) 173.
22. K. J. IRVINE, T. GLADMAN and F. B. PICKERING, *J. Iron Steel Inst.* **199** (1961) 153.
23. R. G. THOMAS and S. R. KEOWN, in Proceedings of the International Conference "Mechanical Behaviour and Nuclear Applications of Stainless Steel at Elevated Temperatures", Varese, Italy (1981) (The Metal Society, London, 1982) Book 280, p. 30.

Received 15 July
and accepted 13 September 1985